Charge transfer and band gap opening of a ferrocene/graphene heterostructure

Bacem Zribi, Anne-Marie Haghiri-Gosnet, Azzedine Bendounan, Abdelkarim Ouerghi, Hafsa Korri-Youssoufi

Charge Transfer and Band Gap Opening of a Ferrocene/Graphene Heterostructure

Bacem Zribi,[a,b] Anne-Marie Haghiri-Gosnet,[b] Azzedine Bendounan,[c] Abdelkarim Ouerghi,[b]

and Hafsa Korri-Youssoufi [a] *

[a] *Institut de Chimie Moleculaires et des Matériaux d'Orsay ICMMO UMR-CNRS 8182, ECBB, University Paris-Sud, Université Paris-Saclay, 420, 91405 Orsay, France.*

[b] *Center of Nanosciences and Nanotechnologies – C2N, UMR-CNRS 9001, Université Paris-Saclay, 10 Boulevard Thomas Gobert, 91120 Palaiseau, France*

[c] *Synchrotron-SOLEIL, Saint-Aubin, BP48, F91192 Gif sur Yvette Cedex, France.*

*Corresponding author, Email: hafsa.korri-youssoufi@u-psud.fr

Abstract

The objective of this paper was to study the electrochemical and electronic behavior of pristine graphene used as a catalyst for redox reactions and the charge transport mechanisms that occur in the interface between graphene and covalently attached ferrocene. The covalent grafting and chemical modification of epitaxial graphene by a ferrocene redox marker was performed through electrochemical oxidation of ethylene diamine that provided a low coverage density and a short distance between the ferrocene and graphene. The electrochemical activity, as well as, the electronic and structural properties of the nanomaterials were characterized by Cyclic Voltammetry, Electrochemical Impedance Spectroscopy, X-ray Photoelectron Spectroscopy , RAMAN spectroscopies and Angle-Resolved-Photoelectron Spectroscopy. We show that the proposed modification improved the electronic properties of graphene where p-doping was observed and a band gap opening of about 60 meV was demonstrated. The electrochemical activity and electron transfer ability was inproved. A heterogeneous electron transfer rate of K_S=7 s^{-1}, was obtained thanks to a low density of immobilzed ferrocene and the small spacer provided by ethylene diamine giving a fast tunneling electron transfer. We believe promising perspectives for the development of self-organized graphene electrodes with various electrochemical properties by tailoring the attached redox functional groups.

Keywords. Graphene, Ferrocene, Electrochemical Patterning, Spectroscopy, Heterostructures.

1. Introduction

Graphene, a two-dimensional (2D) carbon nanomaterial composed of sp^2 hybridized carbon atoms with a honeycomb lattice structure, exhibits excellent electrical and thermal conductivities associated with a high electron mobility[1–7]. Graphene sheets have thus emerged as attractive electrodes for electrochemistry and electro-catalysis due to their exceptional transport properties. They have been used as a biosensing platform by various groups[5–7] for the detection of several biological samples such as DNA, viruses and proteins.[8] Electrochemical sensors with graphene as the transducer [9] are full of promise due to their simplicity and high sensitivity of detection[10], often coupled with low-frequency 1/f noise[11] and a low electron transfer resistance.[12–14] Understanding the mechanisms of electron transfer in such graphene-based biosensing platforms thus appears to be of great importance in this context.

Various studies of electron transfer and surface functionalization have been performed with carbon materials such as glassy carbon electrodes, carbon nanofibers, carbon nanotubes or graphene oxides. Most of these materials present defects in their structure due to the presence of sp^3 structure coming from various levels of oxidation and the presence of oxygen bound to the surface leading to an electrochemical behavior.[9] However, carbon sp^2 nanomaterials such as pristine graphene are known to have low electrochemical properties related to the basal plane and the electron transfer ability is more or less related to the presence of edges[9,15,16] For carbon-based sp^2 nanomaterials, a functionalization based on covalent grafting of a redox marker can enhance electrochemical properties if the redox marker has an electron density at the Fermi level of the nanomaterial.[17]

Among the different functionalization methods for covalent grafting, electrochemical patterning based on diazonium salt reduction[18] or amine oxidation[19] makes it possible to introduce functional groups on the graphene surface for further attachment of biomolecules. Since this type of chemistry depends on the Fermi energy of graphene and the density of states (DOS) of the reagents, the resulting reaction rate depends on the number of graphene layers, defects, and the electrostatic environment. Covalent graphene functionalization can thus enhance the chemical reactivity and the electronic properties of graphene via doping and band-gap engineering.[20] Fewer studies have investigated electron transfer rates through the covalent bonding of a redox marker to graphene-based electrodes. The covalent attachment of ferrocene through click chemistry on a prefunctionalized graphene surface by reduction of a diazonium salt has been demonstrated and gives an electron transfer rate of 0.4 s^{-1}. This low value was attributed to the high density of the polymer layer formed after aryl azide immobilization which increased the distance between the graphene surface and the ferrocene.[18]

For carbon sp^2/sp^3 electrodes such as diamond [21] or graphite, electron transfer of attached ferrocene has been described as a space tunneling mechanism between the redox-active molecule and the surface. In addition, a trade-off between high surface coverage and a fast electron transfer rate exists. In the case of carbon electrodes, the kinetics of electron transfer have been found to be related to conditions of functionalization such as the coverage density and the spacer effects. Thus, the best functionalization approach for applications should be disordered layers with low coverage promoting a high tunneling transfer rate.[21]

The goal of this paper was to study the electrochemical behavior of pristine graphene used as a catalyst for redox reactions as well as the charge transport mechanisms that occur in the interface between graphene and the covalently attached ferrocene.[18][20] We describe that the electrochemical patterning through amine oxidation of ethylene diamine at low oxidation potential range allowed the covalent functionalization of epitaxial graphene and the formation of aminated surface of graphene for further covalent attachment of ferrocene as a redox marker (Figure 1). We demonstrate that this method rendered possible the control of the density of functional groups on the surface and then the density of attached redox molecules. With a reversible and intense redox signal, ferrocene is an ideal "outer sphere" redox system for which the kinetics of electron transfer can be affected by changing the electronic and ionic environments. The graphene/ferrocene heterostructure appears to be a model system for understanding the charge transfer and theits *(?)* effect of the modification upon the electronic properties of graphene.

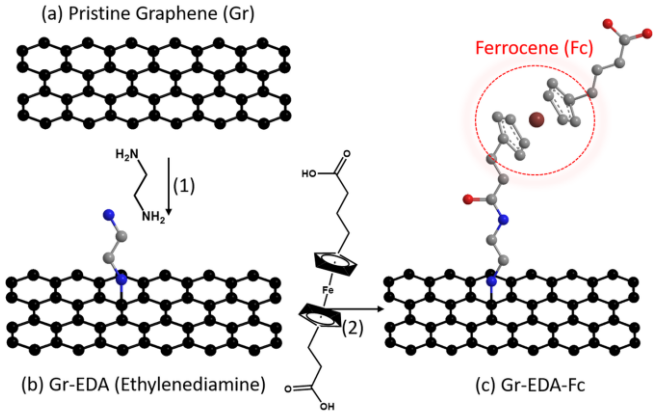

Figure 1. Illustration of the two-step functionalization of the pristine graphene bilayer: a) pristine graphene, b) (EDA) on a graphene bilayer, c) ferrocene- (FC-EDA)- on a graphene bilayer.

The surface coverage of ferrocene (Fc), the kinetic analyses of the charge transfer through the heterogeneous electron transfer rate K_S, and the electrical properties were studied by electrochemical impedance spectroscopy and cyclic volatammetry in order to determine the electrochemical properties of such heterostructures. XPS and RAMAN spectroscopies were also used to analyze the nature of the chemical bonds of the grafted EDA/Fc molecules, as well as the structural and electronic effects of the functionalized bilayer graphene. ARPES was carried out to analyze the electrical properties of graphene and determine how the covalent attachement of the redox marker affected the gap opening and the Fermi velocity.

2. Experimental section

2.1. Chemical reagents

Potassium Ferricyanide(III), Potassium Hexacyanoferrate(II) Trihydrate, Hexaammineruthenium(III) Chloride, Ethylene diamine and Lithium Perchlorate were obtained from Sigma Aldrich. The modified ferrocene group $Fc(NHP)_2$ was synthesized following a procedure described elsewhere.[22] The phosphate buffer solution of 10 mM at pH 7.4 was prepared by mixing stock solutions of NaCl, KCl, Na_2HPO_4, KH_2PO_4 and MilliQ water

(18.25 MΩ.cm). All other chemicals used in the present investigations were commercially available and of analytical reagent grade.

2.2. Preparation of epitaxial graphene

The graphene bilayer was produced via a two-step process beginning with a starting substrate of un-doped 4H-SiC(0001). Firstly, the substrate was hydrogen-etched with 100% H_2 at 1550 °C to produce well-ordered SiC atomic terraces. Subsequently, the SiC sample was heated to 1000°C in a semi-UHV chamber and then further to 1550°C in an Ar atmosphere during 10 min. The graphitization process resulted in the growth of an electrically active graphene layer on top of the buffer layer, covalently bound to the substrate. The sample was then cooled to room temperature and transferred ex-situ to perform the various measurements. [23,24]

The morphology of the graphene sample was observed using Atomic Force Microscopy (AFM) which illustrated a high uniformity on a large-scale surface with the presence of atomically flat terraces. The step direction and the terrace width were fixed by the incidental misorientation of the surface with respect to the crystallographic (0001) plane. The average widths of the (0001) terraces were around 2 µm (see Figure S1).

2.3. Instrumentation

Raman spectroscopy was performed at room temperature with a Renishaw spectrometer, using a 532-nm argon laser focused on the sample with a DMLM Leica microscope with a 100x (NA=0.75) objective. Atomic Force Microscopy (AFM) was used to study the surface morphology in tapping mode using a Veeco Nanoman Dimension V.

The photoemission experiments (XPS, ARPES) were carried out using synchrotron radiation at the TEMPO beamline of the SOLEIL Synchrotron in France. The XPS measurements of the carbon 1s core level were performed at photon energy hν=360 eV and the binding energies were calibrated with respect to the Fermi level. The ARPES data were measured at hν=60 eV with a Scienta SES 2002 electron energy analyzer characterized by high angle and energy resolutions ($\Delta\theta \approx 0.3°$ and $\Delta E \approx 5$ meV at low photon energy).

Electrochemical experiments were realized using the Autolab 30 system equipped with the Nova software. A three-electrode system was used to carry out the electro-chemical studies using epitaxial graphene as the working electrode (0.5 cm^2), bare platinum as the counter electrode and Ag/AgCl as the reference electrode.

2.4. Functionalization of the graphene surface

As shown in Figure 1, the functionalization of pristine graphene with a ferrocene derivative was performed in two steps. The first step consisted in carrying out an optimized functionalization protocol for covalent attachment of ethylene diamine (EDA) molecules on the graphene surface as has previously been described in the case of carbon nanomaterials.[19,25] The optimization of the electrodeposition was performed to overcome the oxidation of graphene and the formation of multiple layers allowing the reaction at a lower potential range. This was performed by an electrochemical reaction through cyclic voltammetry (CV) from 0 to 0.75 V (vs. Ag/Ag/Cl) at a scan rate of 200 $mV \cdot s^{-1}$ during 8 cycles in 1-M EDA solution containing 0.5 M $LiClO_4$/acetonitrile. This electrochemical oxidation reaction produced cationic radicals of ethylene diamine that covalently bound to carbon atoms in the graphene lattice. In the second step, the modified redox marker

ferrocenyl group bearing an activated ester was covalently linked to the aminated surface of graphene without addition of any reagent.[22]

3. Results and Discussion

3.1. Electrochemical characterization of the "Graphene-EDA-Ferrocene" interface

After each functionalization step, the electrochemical properties of graphene were studied using two methods, namely cyclic voltammetry (CV) and electrochemical impedance spectroscopy (EIS). CV analysis in the presence of external redox markers with either inner-sphere or outer-sphere properties was performed to underline both surface and electronic properties of the pristine graphene.[26] This was first done with $[Fe(CN)_6]^{3-/4-}$ as the inner-sphere redox marker where the electron transfer kinetics are dependent not only on the density of electronic states (DOS), but also on the surface microstructure[27]. Secondly, the outer-sphere redox mediator rhuthenium complex $Ru(NH_3)_6^{3+/2+}$ was used, which is insensitive to the surface structure/morpohology and chemistry, and for which the charge transfer depends only on the DOS.

In the first case with $[Fe(CN)_6]^{3/4-}$ as the inner-sphere marker, the electrochemical behavior of graphene before and after functionalization was characterized. A basal plane of graphene with no defects should exhibit poor electrochemical behavior with a flat CV response. The recorded CV with $[Fe(CN)_6]^{3-/4-}$ (Figure 2a – black curve) presented a redox signal with an oxidation and reduction potential at respectively 0.39 and 0.06 V vs. Ag/AgCl and a large peak-to-peak potential separation ΔEp of 332 mV demonstrating a slow, heterogeneous electron transfer at the graphene surface. This behavior is a signature of pristine sp^2 graphene with a high percentage of basal plane as compared to edge plane. It has been proposed that low surface defects such as doping should enhance the electrochemical activity of epitaxial graphene. [28] Thus, the presence of electrochemical activity of graphene could be related to n-type low doping, specifically observed for bilayer graphene on SiC(0001), due to charge transfer from the SiC substrate. [23,24] This behavior was subsequently confirmed through ARPES measurements (see part 3.3).

After EDA grafting, a significant increase in peak current was observed and associated with a large decrease of ΔEp to 127 mV (see SI-2, Fig S2 (b)). This large enhancement of electrochemical activity is characteristic of EDA grafting, as the presence of positively charged amine groups enhances electron transfer of the inner-sphere redox marker $[Fe(CN)_6]^{3-/4-}$. Covalent attachment of ferrocene on the graphene surface underlined a ΔEp of 260 mV with oxidation and reduction potentials at respectively 0.34 and 0.08 V vs. Ag/AgCl, which could be related to the redox couple (attached ferrocene and $[Fe(CN)_6]^{3-/4-}$ in solution). This behavior points at the surface properties of graphene becoming modified by amine groups undergoing covalent reactions with ferrocene through an amide link. The surface properties changed from a positively charged aminated surface to a surface modified with ferrocene groups. However, the ΔEp obtained with graphene/ferrocene was lower than the value for pristine graphene, which demonstrates the effect of the redox ferrocene on the electron transfer ability of the modified graphene sheets.

Similarly, the electronic properties of graphene before and after functionalization with EDA and ferrocene were also studied when using $Ru(NH_3)_6^{3+/2+}$ as the outer-sphere redox probe. ΔEp was approx. 100 mV for pristine graphene (Figure 2b) and remained constant after EDA attachment (see SI-2, Fig S2 (a)). A small increase of 10mV was obtained after ferrocene attachment. The outer-sphere redox system was primarly sensitive to the electronic structure, i.e., to the electronic DOS of the electrode materials. The electronic properties were thus slightly modified after ferrocene attachment.

Figure 2 (c) shows the CV analysis of pristine graphene before and after ferrocene grafting performed in a phosphate buffer solution free of redox species (Figure 2 c). The CV of pristine graphene presented no redox reaction and low background capacitive currents (Figure 2c – black curve) as generally observed[29],[28]. A similar response was obtained with blank tests showing no adsorption of either ferrocene or EDA after the graphene surface was dipped in ferrocene solution or in EDA/ferrocene solution without applying a potential (see SI.3 Figure SI-3). As expected for the grafted ferrocene redox marker, graphene-EDA-Fc (Figure 2c – red curve) exhibited a reversible redox signal of ferrocene with a redox standard potential of 0.26V and high peak current values for both the oxidation and reduction peaks observed at respectively 0.28 and 0.24 V vs. Ag/AgCl. The 40-mV difference in potential between oxidation and reduction peaks demonstrated a well reversible redox signal. The variation of current peaks varied linearly with scan rate demonstrating that the electrochemical process was fully controlled by electron transfer rather than diffusion (see SI-4, Fig. S4).

The ferrocene surface coverage Γ (mol.cm^{-2}) was also estimated from the slopes of the linear plots of the current versus the scan rate, according to the Randles-Sevcik equation:[30]

$$I_P = \frac{n^2 F^2 A \upsilon \Gamma}{4RT}$$

where n represents the number of electrons involved in the reaction (one electron), A is the surface area of the electrode (0.5 cm^2), T is the temperature (300 K), and Γ (mol.cm^{-2}) is the surface coverage.

Γ was determined to be 4.8 ×10^{-11} mol cm^{-2} (~2.9 ×10^{13} molecules cm^{-2}). This value was lower than that of a CVD graphene sheet modified with ferrocene via diazonium chemistry which was estimated to be 4.9 ×10^{-10} mol cm^{-2} [18]. Γ was also lower than the value 4×10^{14} molecules cm^{-2} [31] calculated for a fully packed monolayer of ferrocene. This demonstrated that the electrochemical grafting of EDA led to a less significant surface modification than conventional electrochemical diazonium chemistry.

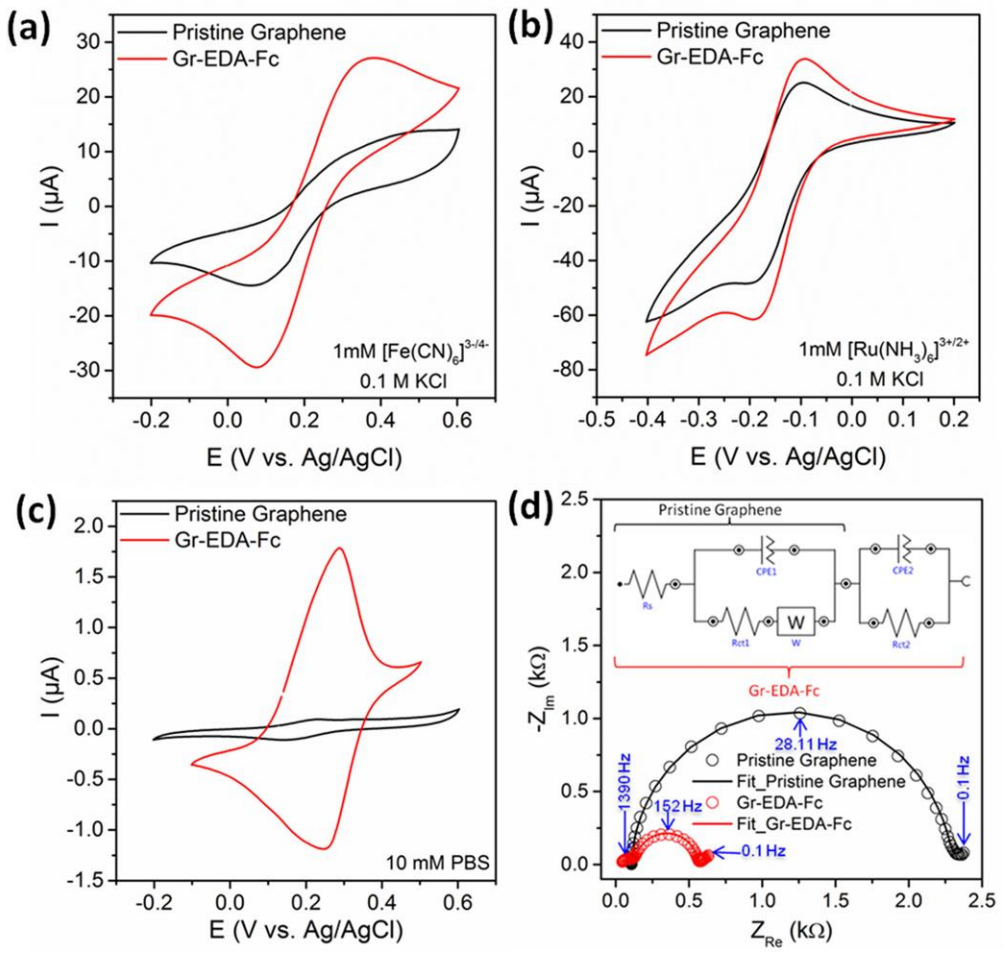

Figure 2. Cyclic voltammograms of pristine graphene (black curve) and Gr-EDA-Fc (red curve) towards (a) $Fe(CN)_6^{3-/4-}$, (b) $Ru(NH_3)_6^{3+/2+}$ and (c) a PBS solution at a scan rate of 50 mVs^{-1}. (d) Nyquist plots obtained in the frequency range from 10 kHz to 0.1 Hz at 0.25 V vs. Ag/AgCl by applying 10 mV (AC mode) in 10-mM $[Fe(CN)_6]^{3/4-}$. The symbols correspond to the experimental data, and the solid lines are the fitted curves using the equivalent circuit shown to the right.

In order to analyze the kinetics of electron transfer of the attached redox ferrocene to the graphene interface, the rate of electron transfer K_S was determined following Laviron's model from the equation: [32]

$$\frac{1}{m} = \frac{nvF}{RT}\frac{1}{K_S}$$

where n is the number of electrons transferred in the redox reaction (n=1), υ is the scan rate, m is the dimensionless rate constant and R, T, F have their usual meanings (see SI-4, inset Fig. S4).

The calculated value of K_S was 7 s^{-1}. This was higher than previous values reported for ferrocene grafted on carbon nanomaterials, where K_S=0.4 s^{-1} for a CVD graphene layer [18], 1 s^{-1} for carbon nanofiber [33], and 1 - 2

s^{-1} for carbon nanotubes [25]. Such a high K_S obtained here demonstrated a fast electron transfer between Fc molecules and graphene and suggests a band-gap opening. Also, K_S could be related to two parameters, first a low-density coverage of ferrocene and secondly the presence of a small spacer between ferrocene and graphene provided by EDA. It has been demonstrated in the case of ferrocene attached to BDD that a high electron transfer ability was favored by low coverage of ferrocene thus preventing steric crowding and favoring tunneling from the bended ferrocene to diamond surface [21]. Similarly, in this study, a small EDA spacer increased the ability of ferrocene to approach the graphene surface and thus enhanced the electron transfer ability.

Electrochemical impedance spectroscopy (EIS) is a characterization tool widely used to study the charge transfer kinetics and to probe the interfacial properties of nanomaterials. The impedance behavior of the graphene electrodes was studied in the presence of the $[Fe(CN)_6]^{3-/4-}$ redox couples that are known as sensitive redox probes to the chemical nature of the carbon electrodes.[34] Figure 2b (black curve) shows the Nyquist plot of a pristine graphene electrode as grown before any functionalization. This plot is divided into two regions, a loop at high frequency and a very small straight line in the low frequency range that corresponds to Warburg diffusion impedance. This very small Warburg component indicates that charge transfer dominates over mass transport effects with a limited diffusion at these ranges of frequency. This circuit was made up of the parallel combination of the Faradaic impedance and the double layer capacitance C_{DL}.

The Faradic impedance is related to the electron transfer of a redox marker through the graphene layer and underlines the intrinsic properties of graphene as a transducer, whereas the capacitance C_{DL} reflects the interfacial properties of the double layer at the graphene/solution interface. This circuit also includes the solution resistance element R_S ($\simeq$100Ω). The semicircle obtained through experimental data was perfectly fitted with the Randels equivalent circuit shown in the inset of Fig. 2d. Hence, the value of each component of the system, namely R_S (the solution resistance), CPE (= C_{DL} that was replaced by a constant phase element CPE known as a pseudo-capacitance), R_{ct} (the charge transfer resistance) and W (the Warburg impedance which represents a semi-infinite diffusion) can be readily obtained using this circuit model. Table S1 (first line) presents the obtained fitted data for graphene (Gr).

The CPE is defined as the relationship of the complex impedance Z' to the angular frequency ω and two additional real parameters, n and T, via the equation $Z' = 1/T(i\omega)^n$. The exponent n is a dimensionless number related to the porosity of the material and non-homogenous distribution of charge, whereas T is a real number that has units defined such that Z' is in ohms. For n= 1, this equation reduces to the expression for the impedance of a perfect capacitor with T equal to the capacitance. In our case, n was about 0.974, a value very close to n= 1 for ideal capacitive behavior. This small shift from ideal capacity can be attributed to a less-homogeneous charge distribution at the "solution/graphene" interface, probably due to the presence of terraces spaced by nanofacets (see SI-1, Figure S1).[12] However, the fact that n was close to 1 confirmed the high crystallinity of the pristine graphene sheet. In addition, the quasi-ideal semi-circle demonstrated that the kinetics were here mainly controlled by charge transfer.[35,36]

Figure 2d (red curve) shows how the ferrocene marker modified the EIS behavior of the layer, giving rise to a large decrease of the diameter of the semi-circle. If the same semi-circle was observed in the corresponding EIS Nyquist plots, the impedance Z_{Re} would decrease after ferrocene immobilization reflecting a decrease of charge transfer resistance from 2.17 KΩ to 428 Ω and a large contribution of redox ferrocene attached to graphene to enhance the electron transfer ability of the external redox marker. This behavior proves the increase of electron transfer ability through the optimized graphene-EDA-Fc electrode. At very high frequency, the Nyquist plot of graphene-EDA-Fc revealed an additional small semi-circle which could be related to the interface properties of the electrode/graphene-ferrocene and reflects the charge transfer through the graphene/ferrocene layer (Figure 2d inset).

The equivalent circuit in this case was formed by a sequence of two parallel circuits, where the phenomenological Rct involved two ways for electron transfer, represented by the charge resistance across the graphene and ferrocene-mediated process (Rct_1 and Rct_2, respectively). Rct comprises a series of sequential steps associated with charge transfer from the redox couple $[Fe(CN)_6]^{3-/4-}$ to Fc (R_{ct1} = 428 Ω) followed by charge transfer from Fc to graphene (R_{ct2}). The electrical parameters are listed in (Table S1, Line 2). The R_{ct2} value related to charge transfer of ferrocene to the graphene electrode showed a very small value of 100 Ω because the charge transfer was entirely channeled through Fc. The apparent heterogenous electron transfer K_{ET} of the external redox marker can be calculated from the impedance data (See SI-4). After ferrocene attachment, the value of K_{ET} increased significantly from 147 s^{-1} to 500 s^{-1} proving the enhancement of the electron transfer ability by attaching ferrocene to the graphene.

One can note that this second circuit gave CPE_2 the value of n=0.74 that is related to a less homogeneous ferrocene distribution in the graphene surface and confirms the results of the CV curve (Figure 2c – red curve) where a large half width was obtained.

To conclude, the electrochemical analysis showed a low coverage Γ of 4.8 $\times 10^{-11}$ mol cm^{-2} of EDA/Fc molecules that were probably grafted on the nanofacets of the graphene terraces. This coverage was associated to a very high value of the heterogeneous charge transfer rate K_S (7 s^{-1}), suggesting a fast electron transfer between the Fc molecules and graphene due to a small band-gap opening.

3.2 Structural analyses of the "Graphene-EDA-Ferrocene" interface using XPS and micro-Raman spectroscopies

Micro-RAMAN spectroscopy was used to depict both structural and electronic properties of the graphene-EDA-Fc heterostructure and explain electrochemical data. Figure 3a shows the micro-RAMAN spectrum in the wavelength range 1200 – 3000 cm^{-1}. Three main bands expected for graphene layers can be seen with the D band at 1360 cm^{-1}, the G band at 1585 cm^{-1} and the 2D band at 2720 cm^{-1}. To study the homogeneity of our sample, different spectra were acquired in diverse areas of the substrate in order to verify the uniformity of the signal. The intensity ratio of the D band represents the density of defects or structural disorder from step edges in graphene. All the recorded spectra exhibited a G/D ratio of about 20, indicating a very low density of defects.

The 2D band observed at 2705 cm^{-1} exhibited a full width half maximum of 50 cm^{-1} indicating the presence of bilayer graphene. In addition, we note the absence of the (G+D) band at 2930 cm^{-1}, corresponding to the disorder-induced feature that is known to occur in sp^2 carbon with defects. The low intensity of the D band, as well as the absence of the (G+D) band, suggests a high crystallinity of the graphene bilayer and the lowest density of defect which confirm the results obtained with electrochemical inner-sphere redox marker $[Fe(CN)_6]^{3-/4-}$.

The D and 2D bands provided information relevant to the transport properties of the samples before and after the functionalization step. Thus, graphene-EDA-Fc (red spectrum in Figure 3a) showed a D band with very low intensity compared to the 2D band and no (G+D) bands were observed at 2930 cm^{-1}, which was first proof of the absence of disorder with a high sp^2 component of the functionalized layer.

This result was the consequence of the soft electrochemical functionalization based on the use of ethylene diamine (EDA) molecules as a chemical spacer and linker to covalently attach Fc to the graphene layer (step 1 – Figure 1). In order to limit the alteration of the electronic properties of graphene during Fc functionalization (Step 2 – Figure 1), this reaction was performed using cyclic voltammetry at low voltage up to 0.75 V (vs. Ag/Ag/Cl) to produce cationic radicals allowing for covalent binding of low amounts of EDA. The low D band of RAMAN spectra confirmed the lowest amount of the EDA molecules, which did not induce disorder in the graphene structure. The top graphene-EDA-Fc layer thus exhibited a high sp^2 component reflecting the soft behavior of the electrochemical functionalization that does not alter the structural properties of pristine graphene. Similar results have been previously reported by Vagin et *al.*[37] showing for the first time that an anodization process can only induce defects in graphene monolayers, not in bilayers.

A low downshift of the 2D peak position by 20 cm^{-1} coupled with a decrease in the FWHM (2D) was here observed after Fc grafting (Figure 3a). Since the FWHM(2D) has been previously shown to be directly correlated to the hole mobility[38]·[39], it reflected an increase in carrier mobility due to an electronic interaction between Fc molecules and graphene. A similar observation for the G band would confirm this hypothesis, but in our data, the G line signal was not strong enough. The graphene-EDA-Fc layer appeared to be doped. This result was in agreement with the electrochemical measurment obtained using the outer-sphere redox probe thus proving a small DOS variation.

To investigate the atomic composition as well as the nature of the chemical bonds, XPS measurements were carried out for the as-grown pristine graphene and the graphene-EDA-Fc, as shown in Figure 3 (graphs (b)). The chemical modification of graphene with EDA introduces aminated-functionalized surface, wherefore it is of great importance to verify the nature of these aminated bonds by XPS (see SI-5, Fig. S5). N_{1s} and O_{1s} peaks could be clearly detected in each zone of the graphene-EDA-Fc sample as the signature of the EDA molecules attached to the graphene (Figure 3b). Subsequently, the redox marker ferrocene was linked covalently to the aminated surface of graphene (step 2 – Figure 1) without addition of any reagent.[22] The XPS scan survey also exhibited two contributions at 720.8 eV and 708 eV, which can be attributed to Fe^{2+} (Fe 2p 3/2) and Fe^{3+} (Fe 2p 1/2) respectively, thereby confirming the presence of ferrocene on the surface. Figure 3c shows a direct

superposition of C_{1s} core level signatures of as-grown pristine graphene and graphene-EDA-Fc with an upwards shift of 0.18 eV. This shift clearly reflects p-doping of the graphene-EDA-Fc due to the presence of Fc.

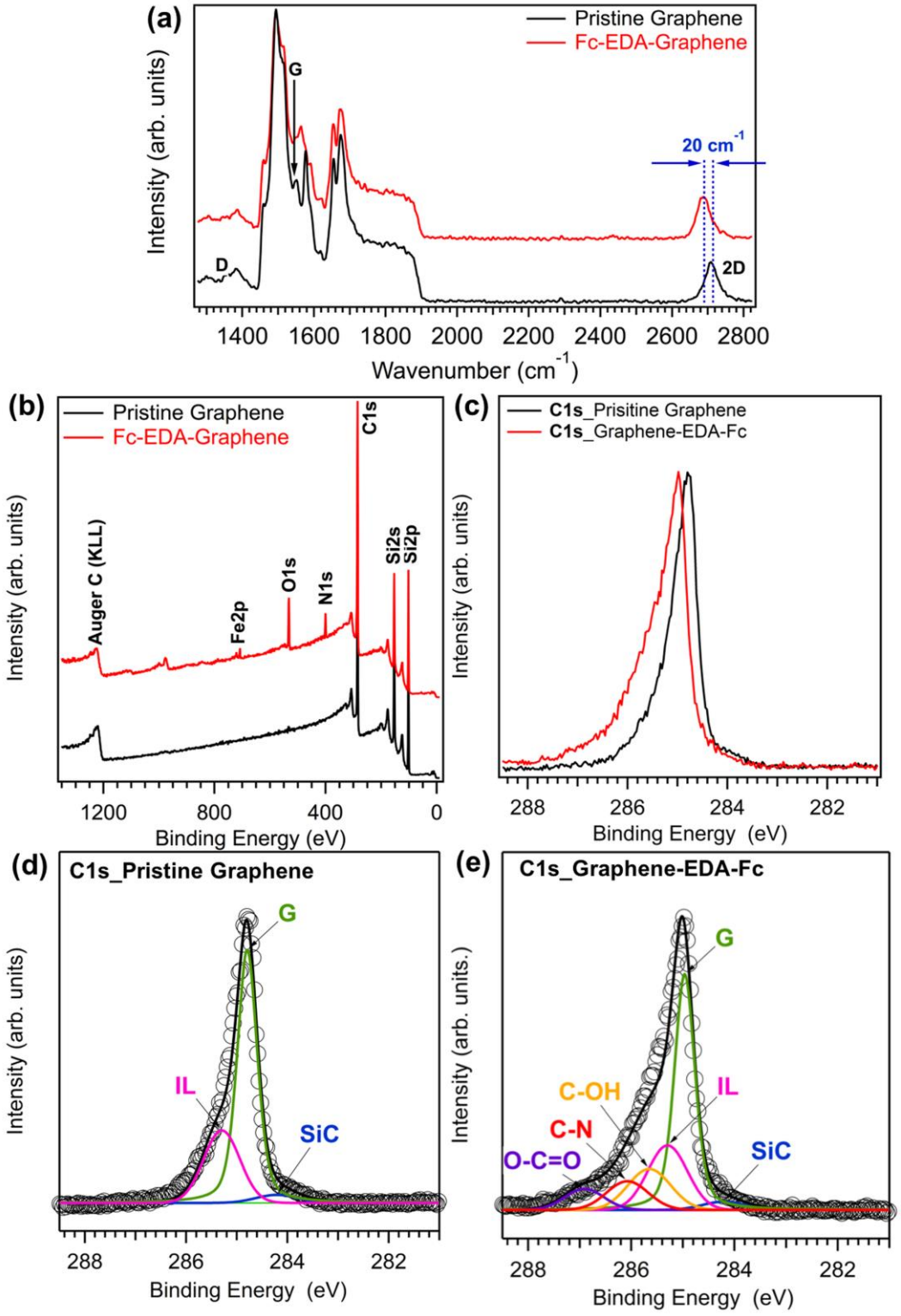

Figure 3. (a) Micro-RAMAN spectra and (b) XPS spectra recorded on the pristine epitaxial graphene on 4H-SiC (0001) before (black line) and after (red line) functionalization of the layer, (c), (d) and (e) C1s XPS spectra for pristine graphene and graphene-EDA-Fc at h γ = 360 eV (surface sensitive). The spectra were fitted using a Shirley-type baseline and Doniach-Sunjic line shape profile, with a Gaussian profile.

To better study the doping effect in graphene, C_{1s} core level signatures were analyzed before (Figure 3d) and after functionalization (Figure 3e). Different components were decomposed using a curve-fitting procedure. The experimental data points are displayed as dots and the black line corresponds to the envelope of the fitted components. The C_{1s} core level spectrum of as-grown pristine graphene (Figure 3d) presents the typical shape of a graphene bilayer grown on SiC(0001). Three peaks were used to fit the original spectra of C1s of pristine graphene, corresponding to SiC (~ 284.21eV), graphene (G ~ 284.89eV) and an interface layer (IL ~ 285.29eV). The intensity of this IL that should decrease with increasing thickness was found to be consistenly close to constant. It corresponds to the first carbon layer partially sp^3 bound to the SiC surface that has no carbon sp^2 properties.[40] The C_{1s} of the graphene-EDA-Fc (Fig. 3 (e)) can be decomposed into six peaks at 284.21, 284.98, 285.28, 285.66, 286.17 and 286.91 eV which can be assigned to SiC, G, IL, C-OH, C-N and O-C=O bonds, respectively. These C-OH, C-N and O-C=O bonds confirmed the presence of EDA-Fc covalently grafted to the graphene surface.

3.2 Band gap measurements using ARPES spectroscopy

To gain further insight into the electronic properties of the functionalized graphene layer and confirm a band gap opening, the role of EDA-Fc covalently grafted molecules on the graphene was studied using Angle Resolved Photoemission Spectroscopy (ARPES) at 60 eV. The band structures of pristine graphene and graphene-EDA-Fc, collected at the K point along the ΓK direction, at room temperature, are shown in Figures 4 a and d, respectively. The band structure was measured before and after deposition of molecules on the bilayer graphene. For the as-grown pristine graphene, the π-band split into two bands, due to an interlayer decoupling, proving that a graphene bilayer was present at the surface. The two branches of the bilayer bands were clearly visualized with the momentum dispersion curves (Figure 4b). Furthermore, the Dirac crossing point of the π band was located around 0.3 eV below the Fermi level with a band gap of about 110 meV.[41] This band gap and n-type low-doping specifically observed for bilayer graphene on SiC(0001) was due to the charge transfer from the SiC substrate. More precisely, this charge transfer coming from the negative charge in the interlayer (IL) occurred due to the dangling bonds between SiC substrate and graphene layer. The Fermi velocity, measured via the slope of linear dispersion, was found to be 1.097×10^6 ms^{-1}, which was in good agreement with the work of.Sprinkle *et al.*[42]. The band gap was also found to increase with the edge plane defects.[43]

For graphene-EDA, the band structure was preserved and the fitting of the linear dispersion slope (see SI-6, Fig. S6) gave a Fermi velocity of about 1.034×10^6 ms^{-1} which was lower than for the pristine graphene (1.097×10^6 ms^{-1}). This confirms previous electrochemistry results on the fact that low quantities of EDA were covalently

bonded keeping the crystallographic structure of the graphene surface without altering their band structure. A similar behavior of Fermi velocity evolution has been observed, for example, for covalent functionalization of graphene by a cycloaddition reaction[44]. This result agreed well with theoritical calculations suggesting that the opening band gap in the electronic structure of graphene could be obtained only for 25% of chemical functionalization sites.[45]

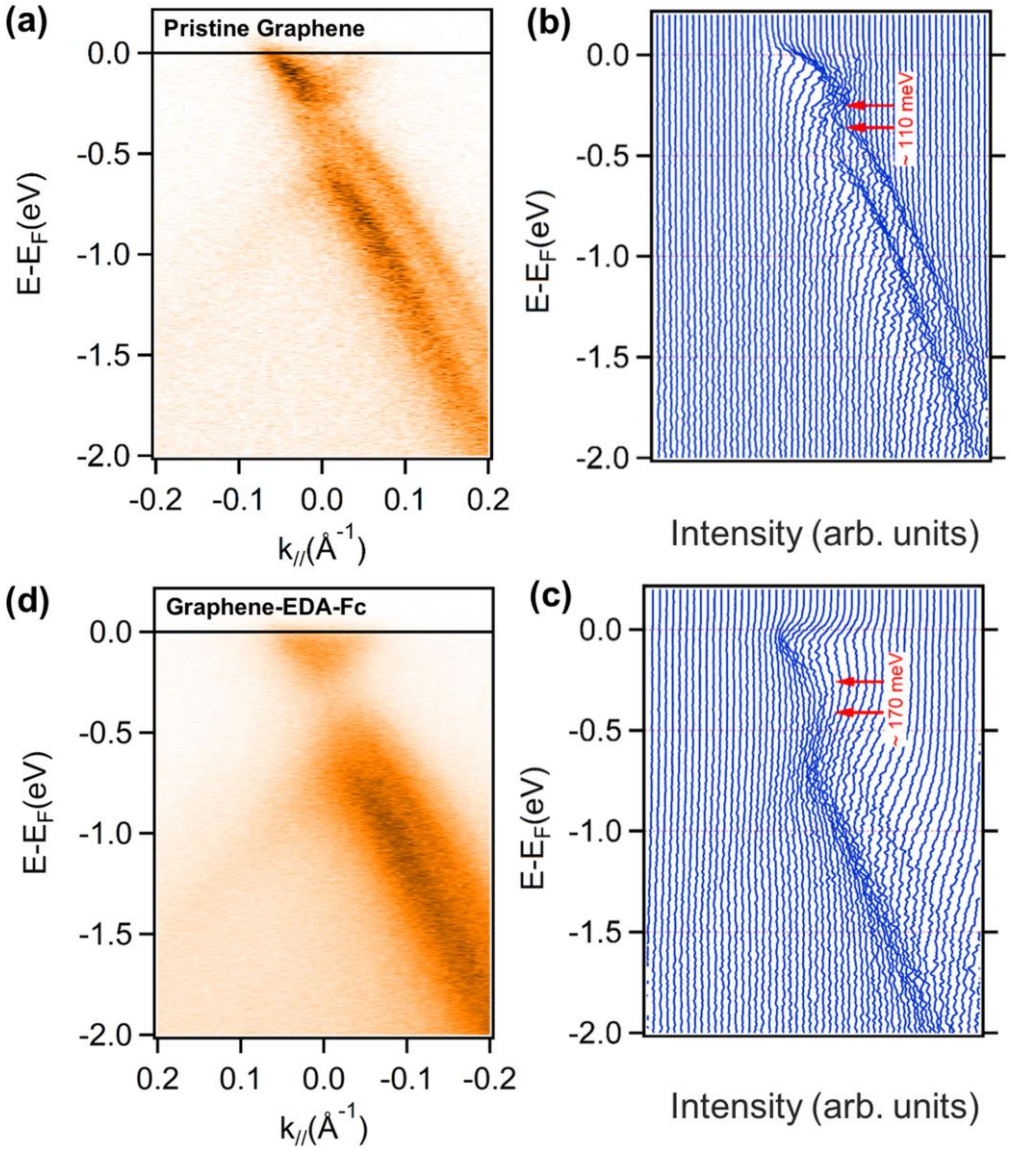

Figure 4. ARPES at room temperature of (a) pristine graphene/SiC(0001) and (d) graphene-EDA-Fc, energy vs. momentum dispersion relation, (b) pristine graphene/SiC(0001) and (c) graphene-EDA-Fc, measured at hν = 60 eV, through the K point, along the ΓK direction at room temperature.

After Fc functionalization of graphene, a tendency for increasing the gap opening to 170 meV was seen compared with the value of pristine graphene which was about 110 meV (Figures 4 c and d). In addition, a Fermi

velocity for the graphene-EDA-Fc was at 1.105 $\times 10^6$ ms^{-1}, close to the pristine graphene. ARPES results confirmed the band-gap opening of the graphene-EDA-Fc heterostructure which originated from the fast tunneling electron transfer from ferrocene molecules to the graphene layer.[21,46] The strategy performed here involved a very low amount of Fc molecules covalently grafted on the graphene bilayer which could generate a local excess of charge inducing a band-gap opening. This led to a selective organic functionalization of graphene without totally disrupting its electronic properties. This should be correlated with the notable properties of ferrocene as an organometallic redox promoter[47] coupled to the electronic structure of graphene.[18]

To evaluate the electronic properties of the samples, the electron density of pristine graphene was also determined before and after ferrocene functionalization. From the ARPES measurements, the energy position at the K point (Dirac Energy E_D) with respect to the Fermi Energy position (E_F) was evaluated.[48] The results obtained show $E_D^{Pristine} \approx 0.3$ eV for the pristine graphene, which corresponds to an electron density value of about 4.6 $\times 10^{12}$ cm^{-2}. For graphene-EDA-Fc, $E_D^{Graphene-EDA-Fc} \approx 0.21$ eV, which corresponds to an electron density value about 1.9 $\times 10^{12}$ cm^{-2}, suggesting an effective electron doping of the graphene despite a low amount of ferrocene dopants. The difference in electron density between the pristine and Fc-doped graphene estimated to be around 2.7 $\times 10^{12}$ cm^{-2} was due to the covalent linking of ferrocene molecules to the graphene layer through small EDA spacers.

4. Conclusion

Electrochemical patterning with small EDA spacers for covalent grafting of ferrocene redox markers on a graphene surface is an elegant way to simultaneously enhance the electrochemical reactivity and the electronic properties of graphene with higher free charge-carrier densities. Experimentally, the electron transfer rate K_S of about 7 s^{-1} measured here is to the best of our knowledge the highest measured value for ferrocene grafted on graphene-based materials. Fast kinetics through the graphene-EDA-Fc interface should also be associated to the low surface coverage Γ of 4.8 $\times 10^{-11}$ mol cm^{-2} (~2.9 $\times 10^{13}$ molecules cm^{-2}) which favors both charge transfer and band gap-opening as clearly observed by XPS/ARPES and by electrochemical measurements using inner-sphere redox markers $Ru(NH_3)_6^{3+/2+}$. Soft electrochemical functionalization through EDA oxidation appeared to be a key parameter, since both structural and electronic properties of graphene seemed not to be altered after functionalization with a major sp^2 component and a Fermi velocity of the charge carriers similar to that of as-grown pristine graphene. Finally, the work reported here should lead to a better understanding of charge transport mechanisms at the interface between graphene and ferrocene. It also opens the way for studying charge transfer mechanisms of others markers and biomarkers for further development of graphene-based surfaces with various functionalities.

Acknowledgments:

The authors' acknolodge University Paris-Sud and CNRS for finding this project and gratuful to Soleil Synchrotron for time accorded for the beam line TEMPO. The project PHC N° 39382RE is acknolodged for suppoting a part of this project.

References

[1] A.K. Geim, K.S. Novoselov, The rise of graphene., Nat. Mater. 6 (2007) 183–191.

[2] B.J. Schultz, R. V Dennis, V. Lee, S. Banerjee, An electronic structure perspective of graphene interfaces., Nanoscale. 6 (2014) 3444–3466.

[3] S. V. Morozov, K.S. Novoselov, M.I. Katsnelson, F. Schedin, D.C. Elias, J. a. Jaszczak, a. K. Geim, Giant intrinsic carrier mobilities in graphene and its bilayer, Phys. Rev. Lett. 100 (2008) 11–14.

[4] D.L. Nika, E.P. Pokatilov, a. S. Askerov, a. a. Balandin, Phonon thermal conduction in graphene: Role of Umklapp and edge roughness scattering, Phys. Rev. B - Condens. Matter Mater. Phys. 79 (2009) 155413 1–42.

[5] J.N. Tiwari, V. Vij, K.C. Kemp, K.S. Kim, Engineered Carbon-Nanomaterial Based Electrochemical Sensors for Biomolecules Engineered Carbon-Nanomaterial Based Electrochemical Sensors for Biomolecules, ACS nano 10 (2015) 46–80.

[6] Y. Liu, X. Dong, P. Chen, Biological and chemical sensors based on graphene materials, Chem. Soc. Rev. 41 (2012) 2283–2307.

[7] W. Yang, K.R. Ratinac, S.R. Ringer, P. Thordarson, J.J. Gooding, F. Braet, Carbon nanomaterials in biosensors: Should you use nanotubes or graphene ?, Angew. Chemie - Int. Ed. 49 (2010) 2114–2138.

[8] S. Ge, F. Lan, F. Yu, J. Yu, Applications of graphene and related nanomaterials in analytical chemistry, New J. Chem. 39 (2015) 2380–2395.

[9] D. a. C. Brownson, D.K. Kampouris, C.E. Banks, Graphene electrochemistry: fundamental concepts through to prominent applications, Chem. Soc. Rev. 41 (2012) 6944–6977.

[10] O. Akhavan, E. Ghaderi, R. Rahighi, Toward single-DNA electrochemical biosensing by graphene nanowalls., ACS Nano. 6 (2012) 2904–16.

[11] A. a Balandin, Low-frequency 1/f noise in graphene devices., Nat. Nanotechnol. 8 (2013) 549–55.

[12] P. Szroeder, N.G. Tsierkezos, M. Walczyk, W. Strupiński, A. Górska-Pukownik, J. Strzelecki, K. Wiwatowski, P. Scharff, U. Ritter, Insights into electrocatalytic activity of epitaxial graphene on SiC from cyclic voltammetry and ac impedance spectroscopy, J. Solid State Electrochem. 18 (2014) 2555–2562.

[13] A. Bonanni, M. Pumera, Graphene Platform for Hairpin-DNA- Based Impedimetric Genosensing, ACS nano 5 (2011) 2356–2361.

[14] A. Bonanni, A.H. Loo, M. Pumera, Graphene for impedimetric biosensing, TrAC - Trends Anal. Chem. 37 (2012) 12–21.

[15] D.K. Kampouris, C.E. Banks, Exploring the physicoelectrochemical properties of graphene, Chem. Commun. 46 (2010) 8986–8988.

[16] D.A.C. Brownson, L.J. Munro, D.K. Kampouris, C.E. Banks, Electrochemistry of graphene: Not such a beneficial electrode material?, RSC Adv. 1 (2011) 978–988.

[17] H. Randriamahazaka, J. Ghilane, Electrografting and Controlled Surface Functionalization of Carbon Based Surfaces for Electroanalysis, Electroanalysis. 28 (2016) 13–26.

[18] P. Fortgang, T. Tite, V. Barnier, N. Zehani, C. Maddi, F. Lagarde, A.-S. Loir, N. Jaffrezic-Renault, C. Donnet, F. Garrelie, C. Chaix, Robust electrografting on self-organized 3D graphene electrodes, ACS Appl. Mater. Interfaces. 8 (2016) 1424–1433.

[19] B. Zribi, J.-M. Castro-Arias, D. Decanini, N. Gogneau, D. Dragoe, A. Cattoni, A. Ouerghi, H. Korri-Youssoufi, A.-M. Haghiri-Gosnet, Large area graphene nanomesh: an artificial platform for edge-electrochemical biosensing at the sub-attomolar level, Nanoscale. (2016) 15479–15485.

[20] M.A. Bissett, S. Konabe, S. Okada, M. Tsuji, H. Ago, M. Chemistry, A. Sciences, Enhanced Chemical Reactivity of Graphene Induced by Mechanical, ACS nano 7 (2013) 10335–10343.

[21] R.E. Ruther, Q. Cui, R.J. Hamers, Conformational disorder enhances electron transfer through alkyl monolayers: Ferrocene on conductive diamond, J. Am. Chem. Soc. 135 (2013) 5751–5761.

[22] H. Korri-Youssoufi, B. Makrouf, Electrochemical biosensing of DNA hybridization by ferrocenyl groups functionalized polypyrrole, Anal. Chim. Acta. 469 (2002) 85–92.

[23] B. Lalmi, J.C. Girard, E. Pallecchi, M. Silly, C. David, S. Latil, F. Sirotti, a Ouerghi, Flower-shaped domains and wrinkles in trilayer epitaxial graphene on silicon carbide., Sci. Rep. 4 (2014) 4066.

[24] E. Pallecchi, F. Lafont, V. Cavaliere, F. Schopfer, D. Mailly, W. Poirier, a Ouerghi, High Electron Mobility in Epitaxial Graphene on 4H-SiC(0001) via post-growth annealing under hydrogen., Sci. Rep. 4 (2014) 4558.

[25] B. Zribi, E. Roy, A. Pallandre, S. Chebil, M. Koubaa, N. Mejri, H. Magdinier Gomez, C. Sola, H. Korri-Youssoufi, A.-M. Haghiri-Gosnet, A microfluidic electrochemical biosensor based on multiwall carbon nanotube / ferrocene for genomic DNA detection of Mycobacterium tuberculosis in clinical isolates., Biomicrofluidics. 10 (2016) 014115 1–12.

[26] R.C. Alkire, P.N. Bartlett, J. Lipkowski, Electrochemistry of Carbon Electrodes, Wiley-VCH, (2015).

[27] R.L. McCreery, Advanced Carbon Electrode Materials for Molecular Electrochemistry, Chem. Rev. 108 (2008) 2646–2687.

[28] C.X. Lim, H.Y. Hoh, P.K. Ang, K.P. Loh, Direct Voltammetric Detection of DNA and pH Sensing on Epitaxial Graphene : An Insight into the Role of Oxygenated Defects, 82 (2010) 7387–7393.

[29] W. Yuan, Y. Zhou, Y. Li, C. Li, H. Peng, J. Zhang, Z. Liu, L. Dai, The edge- and basal-plane-specific electrochemistry of a single-layer graphene sheet, Sci. Rep. 3 (2013) 1–7.

[30] A.J. Bard, L.R. Faulkner, Electrochemical methods : fundamentals and applications, 2nd ed., USA, 2001.

[31] W.A. de Heer, C. Berger, M.E. Itkis, E. Bekyarova, M. Sprinkle, R.C. Haddon, P. Ramesh, Chemical Modification of Epitaxial Graphene: Spontaneous Grafting of Aryl Groups, J. Am. Chem. Soc. 131 (2009) 1336–1337.

[32] E. Laviron, General Expression of the Linear Potential Sweep Voltammogram in the Case of Diffusionless Electrochemical Systems, J. Electroanal. Chem. 101 (1979) 19–28.

[33] E.C. Landis, R.J. Hamers, Covalent Grafting of Ferrocene to Vertically Aligned Carbon Nanofibers: Electron-transfer Processes at Nanostructured Electrodes, J. Phys. Chem. C. 112 (2008) 16910–16918.

[34] P. Chen, R.L. McCreery, Control of electron transfer kinetics at glassy carbon electrodes by specific surface modification, Anal. Chem. 68 (1996) 3958–3965.

[35] E. Dubuisson, Z. Yang, K.P. Loh, Optimizing Label-Free DNA Electrical Detection on Graphene Platform, Anal. Chem. 83 (2011) 2452–2460.

[36] K.S. Kim, Y.M. Um, J.R. Jang, W.S. Choe, P.J. Yoo, Highly sensitive reduced graphene oxide impedance sensor harnessing π-Stacking interaction mediated direct deposition of protein probes, ACS Appl. Mater. Interfaces. 5 (2013) 3591–3598.

[37] M.Y. Vagin, A.N. Sekretaryova, I.G. Ivanov, A. Håkansson, T. Iakimov, M. Syväjärvi, R. Yakimova, I. Lundström, M. Eriksson, Monitoring of epitaxial graphene anodization, Electrochim. Acta. 238 (2017) 91–98.

[38] M. Kim, N.S. Safron, E. Han, M.S. Arnold, P. Gopalan, Electronic Transport and Raman Scattering in Size- Controlled Nanoperforated Graphene, ACS nano 6 (2012) 9846–9854.

[39] J.A. Robinson, M. Wetherington, J.L. Tedesco, P.M. Campbell, X. Weng, J. Stitt, M.A. Fanton, E. Frantz, D. Snyder, B.L. VanMil, G.G. Jernigan, L.M.W. Rachael, C.R. Eddy, D.K. Gaskill, Correlating raman spectral signatures with carrier mobility in epitaxial graphene: A guide to achieving high mobility on the wafer scale, Nano Lett. 9 (2009) 2873–2876.

[40] C. Riedl, C. Coletti, U. Starke, Structural and electronic properties of epitaxial graphene on SiC(0001): a review of growth, characterization, transfer doping and hydrogen intercalation, J. Phys. D. Appl. Phys. 43 (2010) 374009.

[41] T. Ohta, A. Bostwick, T. Seyller, K. Horn, E. Rotenberg, Controlling the Electronic Structure of Bilayer Graphene, Science 313 (2006) 951–954.

[42] M. Sprinkle, D. Siegel, Y. Hu, J. Hicks, A. Tejeda, A. Taleb-Ibrahimi, P. Le Fèvre, F. Bertran, S.

Vizzini, H. Enriquez, S. Chiang, P. Soukiassian, C. Berger, W.A. De Heer, A. Lanzara, E.H. Conrad, First direct observation of a nearly ideal graphene band structure, Phys. Rev. Lett. 103 (2009) 1–4.

[43] D.E. Jiang, B.G. Sumpter, S. Dai, Unique chemical reactivity of a graphene nanoribbon's zigzag edge, J. Chem. Phys. 126 (2007).

[44] L. Daukiya, C. Mattioli, D. Aubel, S. Hajjar-Garreau, F. Vonau, E. Denys, G. Reiter, J. Fransson, E. Perrin, M.L. Bocquet, C. Bena, A. Gourdon, L. Simon, Covalent Functionalization by Cycloaddition Reactions of Pristine Defect-Free Graphene, ACS Nano. 11 (2017) 627–634.

[45] E. Bekyarova, M.E. Itkis, P. Ramesh, R.C. Haddon, Chemical approach to the realization of electronic devices in epitaxial graphene, Phys. Status Solidi - Rapid Res. Lett. 3 (2009) 184–186.

[46] D.M. Adams, L. Brus, C.E.D. Chidsey, S. Creager, C. Creutz, C.R. Kagan, P. V. Kamat, M. Lieberman, S. Lindsay, R. a. Marcus, R.M. Metzger, M.E. Michel-Beyerle, J.R. Miller, M.D. Newton, D.R. Rolison, O. Sankey, K.S. Schanze, J. Yardley, X. Zhu, Charge Transfer on the Nanoscale: Current Status, J. Phys. Chem. B. 107 (2003) 6668–6697.

[47] J.J. Gooding, A. Chou, J. Liu, D. Losic, J.G. Shapter, D.B. Hibbert, The effects of the lengths and orientations of single-walled carbon nanotubes on the electrochemistry of nanotube-modified electrodes, Electrochem. Commun. 9 (2007) 1677–1683.

[48] C. Mathieu, B. Lalmi, T.O. Menteş, E. Pallecchi, A. Locatelli, S. Latil, R. Belkhou, A. Ouerghi, Effect of oxygen adsorption on the local properties of epitaxial graphene on SiC (0001), Phys. Rev. B. 86 (2012) 1–5.